COMPUTER SCIENCE

100,000-spin coherent Ising machine

Toshimori Honjo[1]*, Tomohiro Sonobe[2], Kensuke Inaba[1], Takahiro Inagaki[1], Takuya Ikuta[1], Yasuhiro Yamada[1], Takushi Kazama[3], Koji Enbutsu[3], Takeshi Umeki[3], Ryoichi Kasahara[3], Ken-ichi Kawarabayashi[2], Hiroki Takesue[1]*

Computers based on physical systems are increasingly anticipated to overcome the impending limitations on digital computer performance. One such computer is a coherent Ising machine (CIM) for solving combinatorial optimization problems. Here, we report a CIM with 100,512 degenerate optical parametric oscillator pulses working as the Ising spins. We show that the CIM delivers fine solutions to maximum cut problems of 100,000-node graphs drastically faster than standard simulated annealing. Moreover, the CIM, when operated near the phase transition point, provides some extremely good solutions and a very broad distribution. This characteristic will be useful for applications that require fast random sampling such as machine learning.

INTRODUCTION

With the apparent saturation of the progress in digital computers, new types of computers based on nonsilicon physical systems are highly anticipated. Unlike current digital computers based on Turing machine procedures, these computers use time evolution of physical systems to perform tasks such as speech and image recognition, data mining, and optimization (*1*). On the basis of a computing paradigm of "let physics do computation," they include quantum computers (*2*), quantum annealers (*3*), neural networks (*4*), and reservoir computers (*5*), implemented with various physical systems such as superconducting qubits (*6*, *7*), trapped ions (*8*), and photonics (*9*–*12*). One such computer based on experimental physics that is drawing attention to solve combinatorial optimization problem is the coherent Ising machine (CIM), which uses networks of coherent optical oscillators to simulate the Ising model (*13*–*25*). The use of optical oscillators, whose photon energy is much larger than that of thermal noises in the environment, enables us to realize a physical system to simulate the behavior of low-temperature spins at room temperature. Here, we report a CIM with 100,512 degenerate optical parametric oscillator (DOPO) pulses as an artificial spin network with more than 10 billion spin-spin interactions. In this machine, temporally multiplexed DOPO pulses, born in a nonlinear optical waveguide as squeezed vacuum pulses, circulate in a 5-km fiber cavity, while experiencing digitally assisted mutual interaction and nonlinear amplitude evolution, to search for the lower energy state of the Ising model through the collective phase transition of the 100,000 DOPO pulses. We show that the CIM can deliver fine solutions to maximum cut (MAX CUT) problems of fully connected 100,000-node graphs ~1000 times faster than those obtained with a cutting-edge digital computer, which suggests that the CIM will have an advantage in solving combinatorial optimization problems.

Two fundamentally important and often conflicting aspects of solving complex problems are accuracy and computation time. In particular, solving large-scale combinatorial optimization problems for which exact solutions are not generally known requires that a solution be obtained with a certain accuracy in a limited time. On a practical level, examples of these problems are channel allocation in a mobile communications network (*26*) and object detection in a self-driving car. Many of these tasks are classified as combinatorial optimization. It is known that various types of these problems can be converted to ground-state search problems of the Ising model (*27*) with polynomial resources (*28*, *29*). Recently, many physical systems have been constructed to solve Ising problems in a very short time, including superconducting qubits (*6*), complementary metal-oxide semiconductor devices (*30*), trapped ions (*31*), and nanomagnets (*32*). The CIM, one such "Ising machine," uses DOPOs to represent the Ising spins. A degenerate parametric oscillator is known to be a physical system that undergoes a second-order phase transition (*33*) and has been investigated as a logic element for computers owing to its bistable characteristics (*34*). For physical-system computers, scalability is fundamentally important in obtaining nontrivial evidence of the effectiveness of such computation; however, many of them often fail to scale up because of the difficulty in controlling physical systems. In 2016, our group showed that a CIM could find solutions to a MAX CUT problem of a fully connected 2000-node graph faster than simulated annealing (SA) implemented on a CPU (central processing unit) by a factor of ~50. Here, we report a 100,000-spin CIM, which we believe is the largest physical-system computer ever constructed. Through experiments using the CIM, we provide clear evidence of the CIM's advantage over SA implemented on a cutting-edge CPU in solving problems, which shows the possibility of applying it to combinatorial optimization problems.

RESULTS

Comparison of computation time

The Ising model is a theoretical model describing the behavior of interacting spins. The Hamiltonian of the Ising model is expressed as

$$H = -\sum_{ij} J_{ij}\sigma_i\sigma_j \quad (1)$$

where $\sigma_i = \{-1,1\}$ and J_{ij} denote the value of the ith spin and a coupling coefficient between the ith and jth spins, respectively. The purpose of the Ising machine is to obtain the spin set σ_i to minimize this Hamiltonian for a given J_{ij}. For benchmarking the CIM, we used the MAX CUT problem, which is a graph-partitioning

[1]NTT Basic Research Laboratories, NTT Corporation, 3-1 Morinosato Wakamiya, Atsugi, Kanagawa 243-0198, Japan. [2]National Institute of Informatics, 2-1-2 Hitotsubashi, Chiyoda-ku, Tokyo 101-8430, Japan. [3]NTT Device Technology Laboratories, NTT Corporation, 3-1 Morinosato Wakamiya, Atsugi, Kanagawa 243-0198, Japan.
*Corresponding author. Email: toshimori.honjo.ht@hco.ntt.co.jp (T.H.); hiroki.takesue.km@hco.ntt.co.jp (H.T.)

problem and is known to be a nondeterministic polynomial time–hard combinatorial optimization one. Solving MAX CUT problems is mathematically equivalent to finding the lowest energy state of the Ising model without a magnetic field (details are described in section S6).

First, we compared the computational time of the CIM with that of a current digital computer. For this purpose, we sought a solution to a fully connected 100,000-node graph with 9,999,900,000 undirected edges, which is randomly weighted by {−1, +1}. We generated an instance, which we denote by K100000 hereafter, using a well-known graph generator called Rudy (*35*), whose details are described in section S7.

Because obtaining a solution that can be proved to be the exact solution of this huge problem is impossible in reality, we investigated how to obtain a normative reference score that can be used as a standard for a fine approximate solution. In our previous report (*18*), we used Goemans-Williamson semidefinite programming (GW-SDP) (*36*), which is a relaxation algorithm that theoretically guarantees the solution accuracy. However, a 100,000-node graph is too large to run on GW-SDP because of the long computational time that scales in $\sim O(N^3)$. Therefore, we applied a greedy heuristic algorithm called Sahni-Gonzales (SG), which is known to find approximate solutions to large problems in polynomial time (*37*). Although SG does not guarantee the accuracy of the solution, Okuyama *et al.* have shown that its performance is comparable to that of GW-SDP for large problems (*38*). With SG, which is a deterministic algorithm, we obtained the MAX CUT score of 10,759,955 for K100000. We use this value as the reference score.

We ran MAX CUT of K100000 on the CIM and a digital computer and measured their times to reach the reference score. The pump turn-on schedule of the CIM (schedule 1 in Fig. 1B) was designed to minimize the time to reach the reference score. The amplitudes of the 100,000 DOPO pulses were recorded by the field-programmable gate array (FPGA) system every two circulations in the fiber cavity. The measured amplitude data were transferred to a computer where the score at each circulation was calculated. To evaluate the computation time of the digital computer, we used SA as an algorithm to solve the MAX CUT problems, because it is a general-purpose heuristic algorithm that can be applied to various combinatorial optimization problems and can be straightforwardly scaled up to 100,000-node graphs (*39*). It is known that there are many varieties of modified SA algorithms, each with their pros and cons. In this work, we used the standard SA algorithm, which is widely recognized as a reference algorithm, implemented on a CPU (Intel Core i9-9900K, 3.60 GHz with 64-gigabyte random-access memory). The SA schedule was also adjusted to minimize the time to reach the reference score (details are described in section S10). Figure 2 shows the temporal amplitude evolution of DOPOs observed when we run MAX CUT of K100000, which is an example of the best results obtained when the CIM ran stably. Here, the

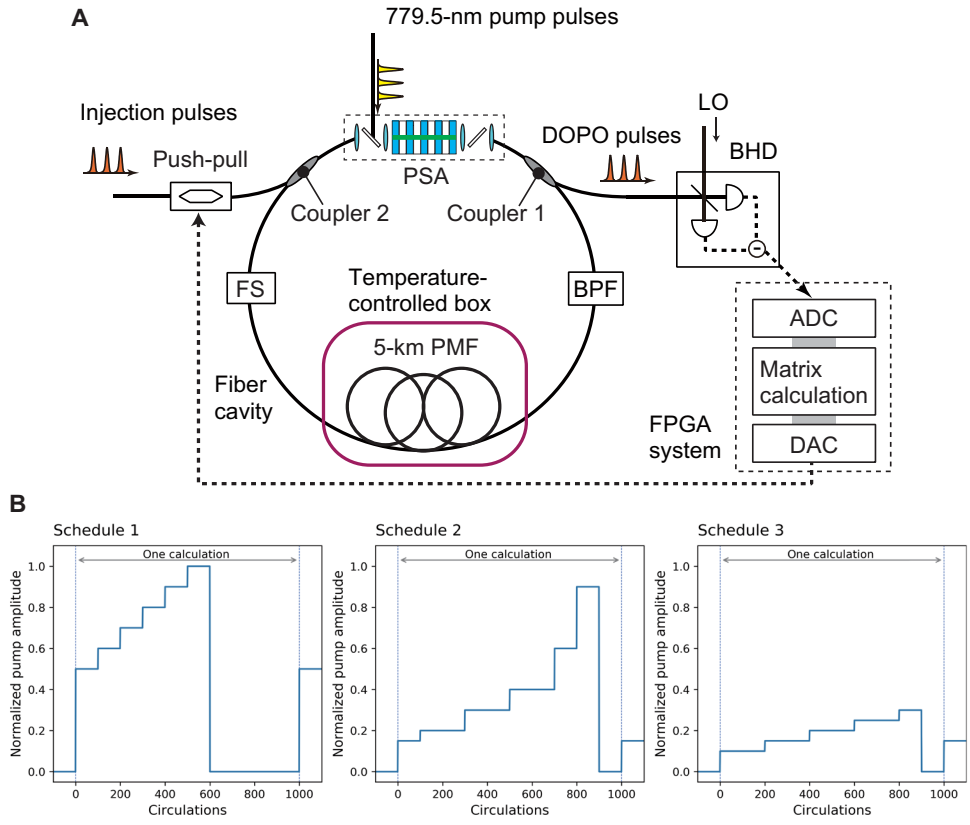

Fig. 1. CIM setup and pump turn-on schedules. (**A**) Experimental setup. The FPGA system includes 56 FPGAs in total (details are explained in section S5). ADC, analog-to-digital converter; BHD, balanced homodyne detector; BPF, band pass filter; DAC, digital-to-analog converter; FS, fiber stretcher; FPGA, field-programmable gate array; LO, local oscillator; PMF, polarization-maintaining fiber; PSA, phase-sensitive amplifier. (**B**) Schedules of the normalized pump amplitude. Schedule 1, pump turn-on schedule designed to minimize the time to reach the reference score; schedules 2 and 3, those for obtaining high scores.

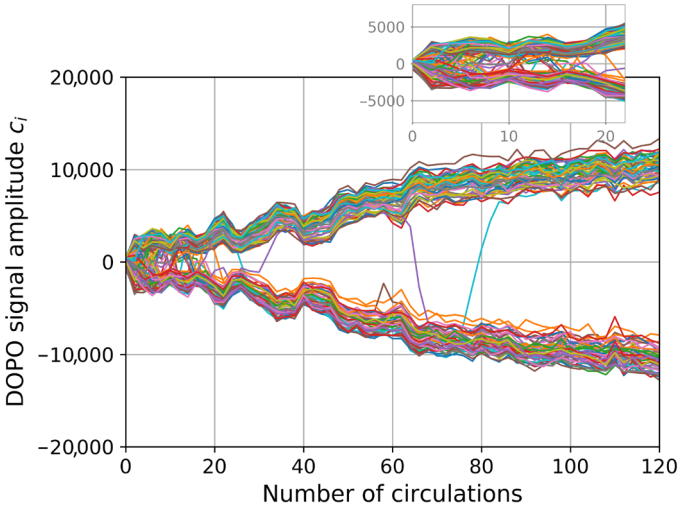

Fig. 2. Amplitude evolution of the first 100 of 100,000 DOPO pulses when running MAX CUT problem of K100000. The unit of the vertical axis is the output of the digital-to-analog converter that digitized the amplitude of the signal from the balanced homodyne detector, where 14 bits (16,384) corresponds to 0.25 V.

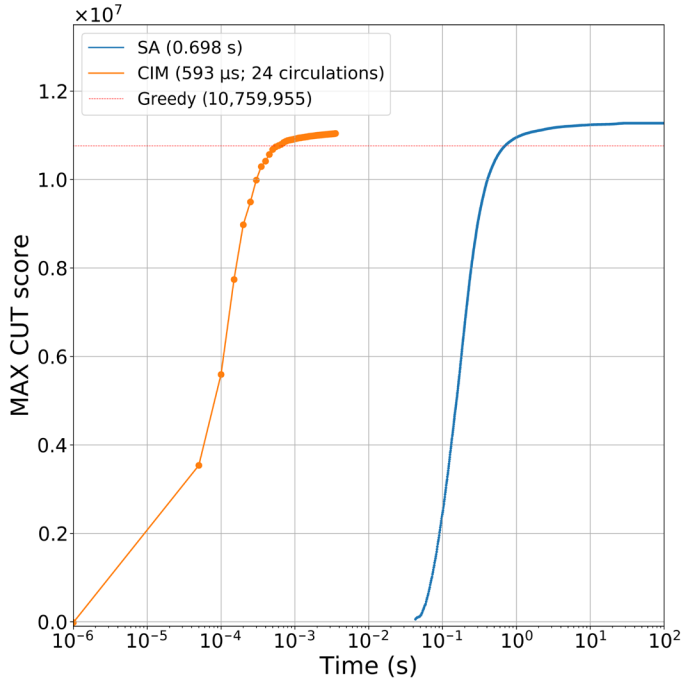

Fig. 3. MAX CUT score as a function of computation time obtained with the CIM (orange line) and SA (blue line). The data points exhibit the scores evaluated at the intermediate steps in the CIM and SA computation. The dotted line denotes the score obtained with SG (10,759,955).

amplitudes of the first 100 of 100,000 DOPO pulses are plotted. The DOPO pulse amplitudes started to grow from noises after the pump was turned on until they saturated at ~100 circulations. The DOPOs exhibited complex dynamics in the first ~20 circulations (see inset of Fig. 2), and then the frequency of sign flips decreased substantially, implying that the search for solutions with lower energy (or higher cut) was mostly undertaken in the first several tens of circulations.

Figure 3 shows the temporal evolution of the cut obtained from the data shown in Fig. 2. The cut rapidly increased at first and then showed saturation, as expected from the trajectory data. The CIM used only 24 circulations to reach the reference score, which corresponds to 593 μs. This result agrees well with a numerical simulation based on c-number stochastic differential equations (CSDEs) with the truncated Wigner approach (see section S8) (*40*). On the other hand, it took 0.698 s for SA to reach the same score, which means that the CIM delivered a solution with the same accuracy ~1000 times faster than SA on a cutting-edge CPU, at least for this particular problem instance.

Scaling in problem size and dependence of edge density

Next, we studied the scaling of the computation time of the CIM and SA on the CPU. We used MAX CUT of complete graphs with sizes of 1000, 10,000, 50,000, and 100,000, which were generated again by Rudy. We ran them on the CIM and SA on the CPU and estimated the average times to reach the reference scores obtained by SG. Again, we used a pump turn-on schedule and an annealing schedule designed to minimize the time to reach the SG score (Fig. 1B, schedule 1). For graphs smaller than 100,000, the present 100,512-spin CIM can embed the same graph multiple times in each run. Therefore, the calculation time was estimated by dividing the time to reach the reference score by the number of embeddings. Note that we can experimentally realize the estimated computation time for the smaller graph by optimizing cavity length. In this way, we took account of the problem size dependence of the optimization of the cavity round-trip time, so that we could avoid overestimating the computation times for smaller graphs. Despite various efforts to stabilize the 5-km fiber cavity (see section S3), the effect of residual instability was still obvious in the measurement of time to reach a reference score. In this measurement, the number of circulations where the DOPO started to rise often fluctuated because of experimental noise in the optical setup, which significantly increased the fluctuation of the computation time more than expected from numerical simulations (see section S8). To evaluate the potential of the CIM, we ran it 500 times and took the average of the top 10 results for each graph. On the other hand, the variance of the calculation time of SA was very small, so we ran SA 10 times and averaged the result.

Figure 4 shows the experimental results. The average computation times of the CIM for 1000- and 100,000-node graphs were 5.43 and 785 μs, respectively, while those of SA were 0.294 and 725.0 ms, which confirm that the difference between the CIM and SA became larger as graph size increased. Figure 4 shows the effective time to reach the SG score as a function of graph size. The result indicates that the computation time of the CIM increased almost linearly, while the scaling of SA became nearly quadratic at graph sizes larger than 10,000. These observations clearly demonstrate that as the node size of the problem increases, the performance gap between the CIM and SA on a CPU widens in terms of computation time. The linear increase of the CIM computation time shown in Fig. 4 means that the number of circulations to reach the reference score was almost constant for all the graph sizes up to 100,000. At present, we cannot deny that the possibility that the CIM operational conditions, such as the pump turn-on schedule and intensity, were not completely optimized, especially for small graphs, which would result in a larger number of circulations required for smaller graphs than

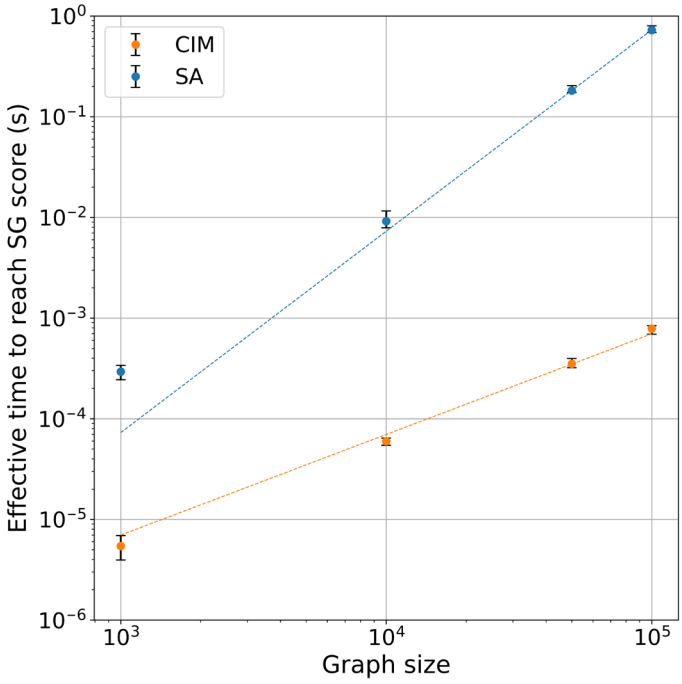

Fig. 4. Effective time to reach the SG score for various graph sizes. The orange (blue) circles show the computation time of the CIM (SA), and the orange (blue) dashed lines are linear (quadratic) auxiliary lines. To estimate the time of CIM, we took the average of the top 10 results of 500 runs.

necessary. Nevertheless, numerical simulations of computations based on oscillator networks also exhibited results similar to those in our experiment (*40*, *41*).

The scaling of SA observed in Fig. 4 can be qualitatively explained as follows. The total number of steps of our SA is basically determined by the number of edges because all the adjacent edges are evaluated for every flip. Thus, the number of steps can be quadratic to the graph size. However, because of other overhead, the calculation time itself is not simply proportional to the number of steps. As one can see in Fig. 4, the data for the 1000- and 10,000-node graphs do not fit well on the quadratic auxiliary line. This is because the overhead of calculating the temperature β and the energy difference ΔE on every loop is not negligible, especially for smaller graphs.

We note here that the present result does not promise similar scaling for higher problem sizes, because of the limited number of experimental data and graph instances used for benchmarking. In addition, a more detailed scaling analysis using time-to-solution for problems with known exact solutions, such as the ones reported in (*42*), will be important future work.

In addition to the scaling of problem size, we also studied the computation time of the CIM for graphs with various densities. We generated 100,000-node graphs with densities of 1, 10, 50, and 100% (details are described in section S7). We ran these graphs on the CIM and estimated the average times to reach the SG scores. For each graph, we operated the CIM 500 times and selected the 10 best scores. Figure 5 shows the experimental results. We observed that the time to reach the SG score was almost the same for all graph densities, which suggests that the CIM computation time to obtain approximate solutions is not dependent on the densities of graphs.

Comparison of solution accuracy

Last, we compared the accuracy of the solutions delivered by the CIM and SA, again using MAX CUT of a K100000 graph. In our experiment to compare computation time, we minimized the time to reach the reference score, whereas, here, we operated the CIM so that it could deliver higher cuts (or lower energy). We increased the number of circulations to 900, during which the pump was increased more slowly than in the experiments described above. We used two pump turn-on schedules, schedules 2 and 3 shown in Fig. 1B. Schedule 2 provides a relatively steep increase in the pump amplitude, while schedule 3 provides a slower increase in its amplitude, with the aim of operating the CIM closer to the oscillation threshold. The DOPO phases were read out at the 890th circulation, which means that the computation time was 22.0 ms. We performed 512 sequential CIM computations, which took 12.6 s in total. To eliminate results where the phases of the injection pulses were inverted, we applied a phase check filter to the data. To eliminate the results where erasure of the phase information from the previous run was incomplete, we also removed the data whose phase configuration exhibited >10% correlation with the previous data (for details of data filtering, see section S9). As a result of the data filtering, we obtained 368 and 231 computation results of 512 for schedules 2 and 3, respectively. To compare the results with the same number of data, we took the first 231 of schedule 2 data. On the other hand, 22 ms is too short for SA to find a solution on the CPU—even the initial energy calculation will not finish within this time. Therefore, we ran SA 231 times with two different computation times, 500 and 1000 ms. The SA schedule was also optimized to obtain higher scores rather than shorter computation time, as described in section S10. Figure 6 shows the histograms of the scores obtained by the CIM and SA, and the scores are summarized in Table 1. The blue and orange columns in Fig. 6 correspond to the results obtained with schedules 2 and 3, respectively. It is apparent that both results with the CIM had peaks in the histogram at larger scores than SA for 1000 ms. In particular, the best and average scores of the CIM with schedule 2 were 11,592,712 and 11,045,206, respectively, both of which are significantly better than those obtained with SA with a computation time ~45 times longer than that of the CIM. Here, note that when we extended the computation time to as long as 1200 s, SA reached a score of 12,032,926, which clearly exceeded that of the CIM. This suggests that, in an application where the allowable calculation time is limited (to ~1 s in MAX CUT of K100000), the CIM has great potential to overwhelm SA in terms of not only computation speed but also solution accuracy. On the other hand, SA still has an advantage in obtaining a better solution if enough computation time is given.

Figure 6 also suggests that the characteristics of the computational results significantly depend on the pump turn-on schedules. It is apparent that schedule 3 provided a broader score distribution than schedule 2. In addition, the best score was obtained with schedule 3. On the other hand, SA recorded better scores with a narrower distribution, which is a typical result obtained with optimization algorithms governed by thermal fluctuations. Although the pump parameter was adiabatically changed with schedule 3 (with a slower pump increase), we observed both a significantly broad score distribution, as shown in Fig. 6, and large fluctuations

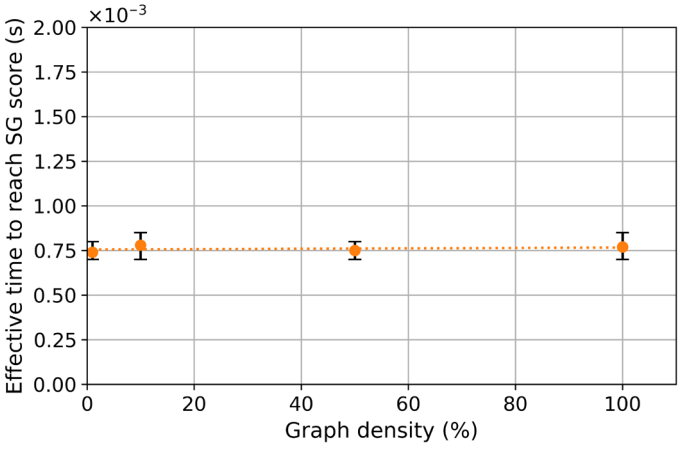

Fig. 5. Time to reach the SG score for 100,000-node graphs with various densities. To estimate the time of CIM, we took the average of the top 10 results of 500 runs.

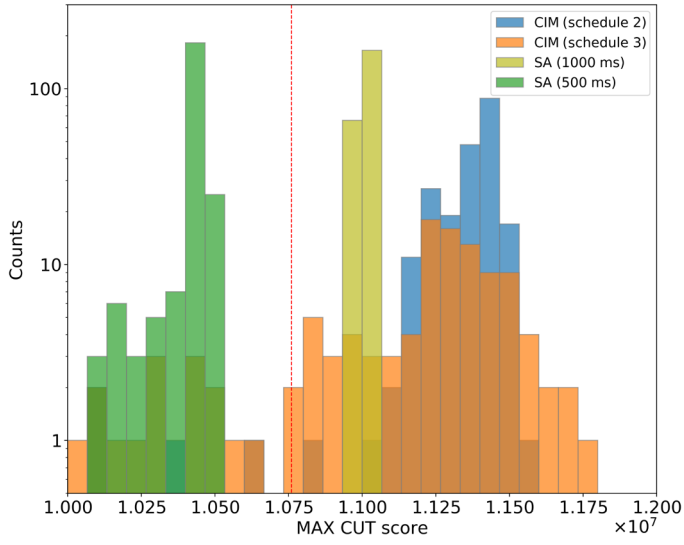

Fig. 6. Histograms of MAX CUT score with CIM and SA. The vertical dashed line shows the SG score (10,759,955).

of DOPO amplitudes, which are detailed in section S9. The broad distribution was probably obtained because the CIM is operated close to the DOPO phase transition point for a long time with the slower pump turn-on schedule, where amplitude fluctuations are strongly enhanced by the collective phase transition of the 100,000 DOPOs. Our hypothesis is that the best score was obtained as a result of critical phenomena observed in a phase transition, such as an elongated correlation length, which may have helped in the search for lower energy states. A broad score distribution with a good best score will be useful for applications that require fast random sampling such as machine learning. We consider that it is hard to reproduce these characteristic distributions obtained near the phase transition for general problem instances with simple numerical simulations using CSDE based on the truncated Wigner approach (*40*).

A natural question is whether we can simulate the CIM operated around the transition point using a more elaborate model. Some of the authors of the present paper are now investigating the solution distribution of the CIM at the transition point using a dissipative quantum model of the CIM dynamics, namely, the Lindblad master equation, derived from a theoretical analysis of the measurement-feedback (MFB) couplings and squeezing with two-body loss on DOPOs. Although there will be no entanglement between DOPOs, this numerical simulation that takes account of factors such as local quantum effects and quantum noises and is resource hungry because of the many-body effects. Therefore, it is hard to simulate large-scale Ising problems with as many as 100,000 spins with the current computational resource available to our team. Nevertheless, they observed a characteristic distribution with simulations based on this model with 10 to 40 spins, which was recently reported in (*43*). At slightly below the transition point, where a random distribution was obtained (as intuitively expected) with the simple CSDE reported in (*40*), this study indicates that the nonclassical fluctuations due to the squeezing and the partial measurement and the feedback process cause a significant broadening in the distribution with a decrease in the mean energy. We hope that the details of the numerical simulations will be published elsewhere in the future.

DISCUSSION

A theoretical paper on an XY Hamiltonian simulator on laser network (*44*) has shown that the probability of obtaining the ground state increases significantly with an adiabatic gain increase. As we described in the preceding section, the CIM result with the adiabatic pump increase exhibited characteristics that are not expected from adiabaticity (the best score was obtained but with a much broader score distribution than those obtained with a steeper pump turn-on schedule), which may be attributed to the behavior at the DOPO critical point, as we discussed above. Further investigating the relationship among adiabaticity, criticality, and energy distribution would be interesting future work.

Whether the dynamical model of a DOPO network can be simulated on the FPGA system is an intriguing question. We expect that the simple truncated Wigner–based CSDEs that we mentioned in the previous section could be implemented on the FPGA system with some additional resources, although the DOPOs' characteristic behavior at around the phase transition point would be hard to simulate with such an implementation.

In the CIM, the time for one computational step, or the time for one circulation in the cavity, increases in proportion to problem size N. On the other hand, although FPGA resources for the matrix computation scale in $O(N^2)$, the time for such a task can scale linearly to the problem size by parallelization, as we have demonstrated with the present FPGA system. Therefore, we believe that the ultimate bottleneck for the computation time results from the time-multiplexing technique used in the generation of DOPO pulses, not from the matrix computation time in an FPGA system. However, in reality, the size and power consumption of an FPGA system will scale in $O(N^2)$, which may practically limit the scalability of the CIM as a computation system.

Recently, inspired by optimization machines based on experimental physics such as quantum annealers and CIMs, researchers have proposed various optimization algorithms and implemented them on digital hardware. These algorithms include those influenced by SA and quantum annealing (*38*, *45*), ones based on the simulation of a classical model of a quantum bifurcation machine

Table 1. Best and mean MAX CUT scores for CIM (schedules 2 and 3, both 21.9 ms), SA (1000 ms), SA (500 ms), and SG.

	Best	Mean
CIM (schedule 2)	11,592,712	11,045,206
CIM (schedule 3)	11,760,078	7,386,632
SA (1000 ms)	11,053,888	11,009,735
SA (500 ms)	10,486,033	10,425,183
SG	10,759,955	10,759,955

(*46*, *47*), and ones based on the modification of stochastic differential equations for describing CIM behavior (*48*, *49*). Some of these "digital Ising machines" have been used to find solutions to 100,000-node class MAX CUT problems. Okuyama *et al.* (*38*) proposed a new algorithm called momentum annealing, which allows us to simultaneously update all spins of fully connected Ising models, and is suitable for parallel implementation on GPUs (graphic processing units). They solved a fully connected 100,000-node graph with a 10-bit weight resolution with four GPUs and showed that the time to reach the SG score was 0.16 s. Goto *et al.* (*46*) proposed a new optimization algorithm simulating adiabatic evolutions of classical nonlinear Hamiltonian systems exhibiting bifurcation phenomena, called simulated bifurcation (SB). They solved a fully connected 100,000-node graph with continuous weight set randomly from −1 to +1. They demonstrated that SB on a GPU-cluster (eight GPUs) reached the score obtained by their Hopfield neural network implementation about 10 times faster than their SA on a PC cluster did. More recently, the same team proposed a modified SB algorithm (*47*), with which a fully connected 100,000-node graph with 10-bit weight resolution was solved. They showed that it can improve the solution accuracy and calculation time compared with the previous SB algorithm (*46*). On another front, various optical Ising machines have also been reported, ranging from large-scale machines based on spatial light modulation with 40,000 spins (*22*) and an opt-electric feedback system with 100 spins (*23*) to small-scale ones using injection-locked multicore fiber lasers (*24*) and integrated DOPOs realized with silicon ring cavities (*25*). It is expected that those digital Ising machines will become practical measures for solving optimization problems in the near future because of their stability, reliability, and low cost compared with nonsilicon physical systems. On the other hand, exploiting analog and nonlinear nature of light may bring new features to computation that are difficult to obtain with digital hardware. Clarifying the advantages and disadvantages of those digital and optical Ising machines, including the CIM, will be important future work for the community.

Although the current CIM still lacks stability and precise controllability of physical parameters, it exhibited promising performance. Moreover, the rich dynamics of coupled optical oscillators in a nonlinear optical medium, as well as the high–signal-to-noise ratio analog computation enabled by high-frequency oscillators realized by optics, are, in principle, hard to simulate with digital hardware. With continuous effort to enable better control of the physical parameters in our system, we believe that the CIM will be the ultimate choice in future computation.

Similar to a laser, our networked DOPO is an open dissipative system, and the simple empirical fact that the mode with the lowest loss is likely to survive in such a system is at the heart of CIM computation. On the other hand, the origin, potential, and limitation of the CIM's computational power have not been clarified yet. The CIM is a physical system with various aspects in that it can be an analog (*48*), a nonlinear (*50*), or an open dissipative system that exhibits nonclassical characteristics (*51*–*53*). We are especially interested in understanding the dynamics of the DOPO network at the oscillation threshold (or critical point), where we experimentally observed interesting score distributions as described above. Clarifying the role of those aspects in the CIM will provide a clue to understanding phase transition phenomena as a resource for future computation.

MATERIALS AND METHODS

CIM with MFB

In our CIM, a DOPO is used to represent the Ising spin. A DOPO is an optical oscillator that uses a phase-sensitive amplifier (PSA) as a gain medium for oscillation. A PSA is realized through a process called signal-idler degenerate optical parametric amplification. In this process, when we input a pump and a signal light into a medium with second- or third-order optical nonlinearity, one quadrature phase component relative to the pump phase is amplified, while the other quadrature component is deamplified. As we increase the pump to the PSA, the system undergoes spontaneous symmetry breaking and then starts to oscillate with either phase 0 or π relative to the pump phase, where the PSA gain becomes maximum. By allocating the phase 0 (π) as a spin-up (spin-down) state, we can stably implement a spin-like system with intrinsic randomness using a high-frequency (~200 THz in our system) optical oscillator. To realize a large-scale CIM, we used time-multiplexed DOPO pulses (*16*) generated in a long fiber cavity (*17*). A schematic of the CIM is shown in Fig. 1A. A PSA based on a periodically poled lithium niobate waveguide (*54*) is placed in the fiber cavity, which also contains an optical bandpass filter, two 90:10 optical couplers, a 5-km polarization-maintaining fiber spool, and a piezo-based fiber stretcher for stabilizing the cavity phase. The cavity round-trip time is 24.7 μs. We input a 779.5-nm pump pulse train at a repetition frequency of 5 GHz into the PSA and, as a result, generate 123,572 time-multiplexed DOPO pulses at the wavelength of 1559.0 nm. A portion of the DOPO pulse energies is split from coupler 1 so that we can measure the quadrature amplitude of the DOPO pulses for each circulation using a balanced homodyne detector (BHD). Among the DOPO pulses, 100,512 pulses are used for the Ising model computation (which we refer to as signal pulses hereafter), while 22,860 pulses are kept oscillating so that we can use them to stabilize the fiber cavity (training pulses), and 100 vacant slots are inserted between the signal and training pulse groups.

We use an MFB scheme (*18*, *19*) to implement flexible interactions among the DOPO pulses. In this scheme, the quadrature amplitude measurement results for the 100,512 signal pulses are input into an FPGA system, which contains 56 FPGAs, an analog-to-digital converter, and a digital-to-analog converter (details are described in section S5). J_{ij}, a 100,512-by-100,512 matrix, for a given Ising model problem is uploaded to the FPGA system in advance. Here, the values of the J_{ij} elements were limited to {−1,0,1} in the present experiment. The FPGA system performs matrix calculation $r_i = \sum_j J_{ij} \tilde{c}_j$, where $\tilde{c}_j$ denotes the BHD measurement result for the jth pulse. We then modulate an optical pulse whose

wavelength is set to exactly the same as that of the DOPO pulses by using a feedback signal $f_i = ar_i$, where a is a constant to determine the coupling strength adjusted by an internal gain parameter in the FPGA system and the amplitude of the pulse. The pulse that carries the feedback signal f_i is input into the ith DOPO pulse through coupler 2 to complete the spin-spin interaction. As a result, we can realize an Ising machine that can simulate 100,512 fully connectable Ising spins, where the total number of two-body interactions amounts to more than 10 billion (10,102,561,632) if we take directional interactions into account. In the computation of the Ising model, we periodically turn the PSA on and off by modulating the pump amplitude while performing the MFB. After we turn the PSA on by injecting the 779.5-nm pump pulses, the PSA emits squeezed vacuum pulses. Those noise pulses circulate in the fiber cavity while undergoing synchronous phase-sensitive amplification and MFB. As the pulse amplitudes increase, gain saturation in the PSA induces competition between the DOPO phase configurations, which helps configurations with the lowest loss, which corresponds to the approximate ground-state energy, to survive with a high probability. We read out the spin value by taking the sign of the DOPO pulse amplitudes after amplitude evolution.

SUPPLEMENTARY MATERIALS

Supplementary material for this article is available at https://science.org/doi/10.1126/sciadv.abh0952

REFERENCES AND NOTES

1. S. Basu, R. E. Bryant, G. de Micheli, T. Theis, L. Whitman, Nonsilicon, non-von Neumann computing—Part I [scanning the issue]. *Proc. IEEE* **107**, 11–18 (2019).
2. P. W. Shor, Algorithms for quantum computation: Discrete logarithm and factoring, in *Proceedings of the 35th Annual Symposium on Foundations of Computer Science*, IEEE, Santa Fe, NM, USA, 20 to 22 November 1994.
3. T. Kadowaki, H. Nishimori, Quantum annealing in the transverse Ising model. *Phys. Rev. E* **58**, 5355–5363 (1998).
4. J. J. Hopfield, D. W. Tank, Computing with neural circuits: A model. *Science* **233**, 625–633 (1986).
5. H. Jaeger, H. Haas, Harnessing nonlinearity: Predicting chaotic systems and saving energy in wireless communication. *Science* **304**, 78–80 (2004).
6. M. W. Johnson, M. H. S. Amin, S. Gildert, T. Lanting, F. Hamze, N. Dickson, R. Harris, A. J. Berkley, J. Johansson, P. Bunyk, E. M. Chapple, C. Enderud, J. P. Hilton, K. Karimi, E. Ladizinsky, N. Ladizinsky, T. Oh, I. Perminov, C. Rich, M. C. Thom, E. Tolkacheva, C. J. S. Truncik, S. Uchaikin, J. Wang, B. Wilson, G. Rose, Quantum annealing with manufactured spins. *Nature* **473**, 194–198 (2011).
7. F. Arute, K. Arya, R. Babbush, D. Bacon, J. C. Bardin, R. Barends, R. Biswas, S. Boixo, F. G. S. L. Brandao, D. A. Buell, B. Burkett, Y. Chen, Z. Chen, B. Chiaro, R. Collins, W. Courtney, A. Dunsworth, E. Farhi, B. Foxen, A. Fowler, C. Gidney, M. Giustina, R. Graff, K. Guerin, S. Habegger, M. P. Harrigan, M. J. Hartmann, A. Ho, M. Hoffmann, T. Huang, T. S. Humble, S. V. Isakov, E. Jeffrey, Z. Jiang, D. Kafri, K. Kechedzhi, J. Kelly, P. V. Klimov, S. Knysh, A. Korotkov, F. Kostritsa, D. Landhuis, M. Lindmark, E. Lucero, D. Lyakh, S. Mandrá, J. R. McClean, M. McEwen, A. Megrant, X. Mi, K. Michielsen, M. Mohseni, J. Mutus, O. Naaman, M. Neeley, C. Neill, M. Y. Niu, E. Ostby, A. Petukhov, J. C. Platt, C. Quintana, E. G. Rieffel, P. Roushan, N. C. Rubin, D. Sank, K. J. Satzinger, V. Smelyanskiy, K. J. Sung, M. D. Trevithick, A. Vainsencher, B. Villalonga, T. White, Z. J. Yao, P. Yeh, A. Zalcman, H. Neven, J. M. Martinis, Quantum supremacy using a programmable superconducting processor. *Nature* **574**, 505–510 (2019).
8. D. Leibfried, R. Blatt, C. Monroe, D. Wineland, Quantum dynamics of single trapped ions. *Rev. Mod. Phys.* **75**, 281–324 (2003).
9. P. Kok, W. J. Munro, K. Nemoto, T. C. Ralph, J. P. Dowling, G. J. Milburn, Linear optical quantum computing with photonic qubits. *Rev. Mod. Phys.* **79**, 135–174 (2007).
10. Y. Shen, N. C. Harris, S. Skirlo, M. Prabhu, T. Baehr-Jones, M. Hochberg, X. Sun, S. Zhao, H. Larochelle, D. Englund, M. Soljačić, Deep learning with coherent nanophotonic circuits. *Nat. Photonics* **11**, 441–446 (2017).
11. L. Larger, M. C. Soriano, D. Brunner, L. Appeltant, J. M. Gutierrez, L. Pesquera, C. R. Mirasso, I. Fischer, Photonic information processing beyond Turing: An optoelectronic implementation of reservoir computing. *Opt. Express* **20**, 3241–3249 (2012).
12. F. Duport, B. Schneider, A. Smerieri, M. Haelterman, S. Massar, All-optical reservoir computing. *Opt. Express* **20**, 22783–22795 (2012).
13. S. Utsunomiya, K. Takata, Y. Yamamoto, Mapping of Ising models onto injection-locked laser systems. *Opt. Express* **19**, 18091–18108 (2011).
14. M. Nixon, E. Ronen, A. A. Friesem, N. Davidson, Observing geometric frustration with thousands of coupled lasers. *Phys. Rev. Lett.* **110**, 184102 (2013).
15. Z. Wang, A. Marandi, K. Wen, R. L. Byer, Y. Yamamoto, Coherent Ising machine based on degenerate optical parametric oscillators. *Phys. Rev. A* **88**, 063853 (2013).
16. A. Marandi, Z. Wang, K. Takata, R. L. Byer, Y. Yamamoto, Network of time-multiplexed optical parametric oscillators as a coherent Ising machine. *Nat. Photonics* **8**, 937–942 (2014).
17. T. Inagaki, K. Inaba, R. Hamerly, K. Inoue, Y. Yamamoto, H. Takesue, Large-scale Ising spin network based on degenerate optical parametric oscillators. *Nat. Photonics* **10**, 415–419 (2016).
18. T. Inagaki, Y. Haribara, K. Igarashi, T. Sonobe, S. Tamate, T. Honjo, A. Marandi, P. L. McMahon, T. Umeki, K. Enbutsu, O. Tadanaga, H. Takenouchi, K. Aihara, K. Kawarabayashi, K. Inoue, S. Utsunomiya, H. Takesue, A coherent Ising machine for 2000-node optimization problems. *Science* **354**, 603–606 (2016).
19. P. L. McMahon, A. Marandi, Y. Haribara, R. Hamerly, C. Langrock, S. Tamate, T. Inagaki, H. Takesue, S. Utsunomiya, K. Aihara, R. L. Byer, M. M. Fejer, H. Mabuchi, Y. Yamamoto, A fully programmable 100-spin coherent Ising machine with all-to-all connections. *Science* **354**, 614–617 (2016).
20. F. Böhm, T. Inagaki, K. Inaba, T. Honjo, K. Enbutsu, T. Umeki, R. Kasahara, H. Takesue, Understanding dynamics of coherent Ising machines through simulation of large-scale 2D Ising models. *Nat. Commun.* **9**, 5020 (2018).
21. R. Hamerly, T. Inagaki, P. L. McMahon, D. Venturelli, A. Marandi, T. Onodera, E. Ng, C. Langrock, K. Inaba, T. Honjo, K. Enbutsu, T. Umeki, R. Kasahara, S. Utsunomiya, S. Kako, K. Kawarabayashi, R. L. Byer, M. M. Fejer, H. Mabuchi, D. Englund, E. Rieffel, H. Takesue, Y. Yamamoto, Experimental investigation of performance differences between coherent Ising machines and a quantum annealer. *Sci. Adv.* **5**, eaau0823 (2019).
22. D. Pierangeli, G. Marcucci, C. Conti, Large-scale photonic Ising machine by spatial light modulation. *Phys. Rev. Lett.* **122**, 213902 (2019).
23. F. Böhm, G. Verschaffelt, G. Van der Sande, A poor man's coherent Ising machine based on opto-electronic feedback systems for solving optimization problems. *Nat. Commun.* **10**, 3538 (2019).
24. M. Babaeian, D. T. Nguyen, V. Demir, M. Akbulut, P.-A. Blanche, Y. Kaneda, S. Guha, M. A. Neifeld, N. Peyghambarian, A single shot coherent Ising machine based on a network of injection-locked multicore fiber lasers. *Nat. Commun.* **10**, 3516 (2019).
25. Y. Okawachi, M. Yu, J. K. Jang, X. Ji, Y. Zhao, B. Y. Kim, M. Lipson, A. L. Gaeta, Demonstration of chip-based coupled degenerate optical parametric oscillators for realizing a nanophotonic spin-glass. *Nat. Commun.* **11**, 4119 (2020).
26. H. Ito, Y. Murata, K. Kurasawa, M. Jing, H. Yasuda, H. Takesue, K. Aihara, M. Hasegawa, Application of Quantum Neural Network to Resource Assignment Problems in Wireless Communication, MITA2019 (2019).
27. E. Ising, Beitrag zur theorie des ferromagnetismus. *Z. Phys.* **31**, 253–258 (1925).
28. F. Barahona, On the computational complexity of Ising spin glass models. *J. Phys. A* **15**, 3241–3253 (1982).
29. A. Lucus, Ising formulations of many NP problems. *Front. Phys.* **2**, 5 (2014).
30. M. Yamaoka, C. Yoshimura, M. Hayashi, T. Okuyama, H. Aoki, H. Mizuno, A 20k-spin Ising chip to solve combinatorial optimization problems with CMOS annealing. *IEEE J. Solid-State Circuits* **51**, 303–309 (2015).
31. K. Kim, M.-S. Chang, S. Korenblit, R. Islam, E. E. Edwards, J. K. Freericks, G.-D. Lin, L.-M. Duan, C. Monroe, Quantum simulation of frustrated Ising spins with trapped ions. *Nature* **465**, 590–593 (2010).
32. B. Sutton, K. Y. Camsari, B. Behin-Aein, S. Datta, Intrinsic optimization using stochastic nanomagnets. *Sci. Rep.* **7**, 44370 (2017).
33. J. Woo, R. Landauer, Fluctuations in a parametrically excited subharmonic oscillator. *IEEE J. Quantum Electron.* **7**, 435–440 (1971).
34. E. Goto, The parametron, a digital computing element which utilizes parametric oscillation. *Proc. IRE* **47**, 1304–1316 (1959).
35. G. Rinaldy, rudy graph generator (1996); https://bit.ly/3CEL7L3.
36. M. X. Goemans, D. P. Williamson, Improved approximation algorithms for maximum cut and satisfiability problems using semidefinite programming. *J. ACM* **42**, 1115–1145 (1995).
37. S. Kahruman, E. Kolotoglu, S. Butenko, I. V. Hicks, On greedy construction heuristics for the MAX CUT problem. *Int. J. Comput. Sci. Eng.* **3**, 211–218 (2007).
38. T. Okuyama, T. Sonobe, K. Kawarabayashi, M. Yamaoka, Binary optimization by momentum annealing. *Phys. Rev. E* **100**, 012111 (2019).
39. S. Kirkpatrick, C. D. Gelatt Jr., M. P. Vecchi, Optimization by simulated annealing. *Science* **220**, 671–680 (1983).
40. Y. Haribara, S. Utsunomiya, K. Kawarabayashi, Y. Yamamoto, A coherent Ising machine for MAX-CUT problems: Performance evaluation against semidefinite programming relaxation and simulated annealing. arXiv:1501.07030 [quant-ph] (28 January 2015).

41. T. Wang, J. Roychowdhury, Oscillator-based Ising machine. arXiv:1709.08102 [cs.ET] (23 September 2017).
42. M. Kowalsky, T. Albash, I. Hen, D. A. Lidar, 3-regular 3-XORSAT planted solutions benchmark of classical and quantum heuristic optimizers. arXiv: 2103.08464 [quant-ph] (15 March 2021).
43. Y. Yamada, K. Inaba, Dissipative quantum dynamics in coherent Ising machine with measurement-feedback spin-spin coupling, Adiabadic Quantum Computing (AQC) 2021, Day 1, Poster B2 (2021).
44. M. Honari-Latifpour, M. A. Miri, Mapping the XY Hamiltonian onto a network of coupled lasers. *Phys. Rev. Res.* **2**, 043335 (2020).
45. M. Aramon, G. Rosenberg, E. Valiante, T. Miyazawa, H. Tamura, H. G. Katzgraber, Physics-inspired optimization for quadratic unconstrained problems using a digital annealer. *J. Math. Phys.* **59**, 062106 (2018).
46. H. Goto, K. Tatsumura, A. R. Dixon, Combinatorial optimization by simulating adiabatic bifurcations in nonlinear Hamiltonian systems. *Sci. Adv.* **5**, eaav2372 (2019).
47. H. Goto, K. Endo, M. Suzuki, Y. Sakai, T. Kanao, Y. Hamakawa, R. Hidaka, M. Yamasaki, K. Tatsumura, High-performance combinatorial optimization based on classical mechanics. *Sci. Adv.* **7**, eaav7953 (2021).
48. T. Leleu, Y. Yamamoto, P. L. McMahon, K. Aihara, Destabilization of local minima in analog spin systems by correction of amplitude heterogeneity. *Phys. Rev. Lett.* **122**, 040607 (2019).
49. E. S. Tiunov, A. E. Ulanov, A. I. Lvovsky, Annealing by simulating the coherent Ising machine. *Opt. Express* **27**, 10288–10295 (2019).
50. T. Leleu, Y. Yamamoto, S. Utsunomiya, K. Aihara, Combinatorial optimization using dynamical phase transitions in driven-dissipative systems. *Phys. Rev. E* **95**, 022118 (2017).
51. K. Takata, S. Utsunomiya, Y. Yamamoto, Quantum correlation in degenerate optical parametric oscillators with mutual injections. *Phys. Rev. A* **92**, 043821 (2015).
52. A. Yamamura, K. Aihara, Y. Yamamoto, Quantum model for coherent Ising machines: Discrete-time measurement feedback formulation. *Phys. Rev. A* **96**, 053834 (2017).
53. T. Shoji, K. Aihara, Y. Yamamoto, Quantum model for coherent Ising machines: Stochastic differential equations with replicator dynamics. *Phys. Rev. A* **96**, 053833 (2017).
54. T. Umeki, O. Tadanaga, A. Takada, M. Asobe, Phase sensitive degenerate parametric amplification using directly-bonded PPLN ridge waveguides. *Opt. Express* **19**, 6326–6332 (2011).
55. T. Kashiwazaki, K. Enbutsu, T. Kazama, O. Tadanaga, T. Umeki, R. Kasahara, Over-30-dB phase-sensitive amplification using a fiber-pigtailed PLLN waveguide module, in *Proceedings of Nonlinear Optics (NLO)* (Optical Society of America, 2019), pp. NW3A.2.
56. A. Marandi, N. C. Leindecker, K. L. Vodopyanov, R. L. Byer, All-optical quantum random bit generation from intrinsically binary phase of parametric oscillators. *Opt. Express* **20**, 19322–19330 (2012).
57. S. V. Isakov, I. N. Zintchenko, T. F. Rønnow, M. Troyer, Optimised simulated annealing for Ising spin glasses. *Comput. Phys. Commun.* **192**, 265–271 (2015).

Acknowledgments: We thank Y. Yamamoto, K. Inoue, K. Igarashi, and S. Utsunomiya for fruitful discussions and H. Tamura for administrative support in this research. **Funding:** This work was funded, in part, by the ImPACT Program of the Council for Science, Technology and Innovation (Cabinet Office, Government of Japan). T.S. and K.-i.K. acknowledge JSPS Kakenhi grant no. JP18H05291 and the Japanese MEXT Quantum Leap Flagship Program (MEXT Q-LEAP), grant no. JPMXS0118069605. **Author contributions:** H.T. proposed the project. T.H. designed the FPGA system. T.H. and H.T. performed CIM experiments. T.In., T.Ik., T.H., and H.T. contributed to bulilding the CIM. K.I. and Y.Y. performed data analyses and numerical simulations. T.K., K.E., T.U., and R.K. fabricated the PPLN waveguide modules. T.S. and K.-i.K. performed the SA benchmark on the CPU. H.T., T.H., and K.I. wrote the manuscript with inputs from all authors. **Competing interests:** T.H., T.In., and H.T. are inventors on patent JP6429346 awarded in November 2018 to the National Institute of Informatics (NII), NTT, and Osaka University, which covers an OPO pulse sequence for calculation and stabilization of a CIM. H.T. is the inventor on patent US10140580 awarded in November 2018 to NII and NTT that covers a CIM using measurement feedback. H.T., K.I., T.In., and T.H. are inventors on patent application PCT/JP2018/038994 submitted by NTT that covers a phase checking scheme for the CIM. T.U. and K.E. are inventors on patent JP5856083 awarded in February 2016 to NTT that covers PSAs based on periodically poled lithium niobate waveguides. The authors declare that they have no other competing interests. **Data and materials availability:** All data needed to evaluate the conclusions in the paper are present in the paper and/or the Supplementary Materials. The SA codes are deposited in Zenodo: https://zenodo.org/record/5153001.

Submitted 16 February 2021
Accepted 4 August 2021
Published 29 September 2021
10.1126/sciadv.abh0952

Citation: T. Honjo, T. Sonobe, K. Inaba, T. Inagaki, T. Ikuta, Y. Yamada, T. Kazama, K. Enbutsu, T. Umeki, R. Kasahara, K.-i. Kawarabayashi, H. Takesue, 100,000-spin coherent Ising machine. *Sci. Adv.* **7**, eabh0952 (2021).

ScienceAdvances

100,000-spin coherent Ising machine

Toshimori HonjoTomohiro SonobeKensuke InabaTakahiro InagakiTakuya IkutaYasuhiro YamadaTakushi KazamaKoji EnbutsuTakeshi UmekiRyoichi KasaharaKen-ichi KawarabayashiHiroki Takesue

Sci. Adv., 7 (40), eabh0952. • DOI: 10.1126/sciadv.abh0952